Anomalous Small-Angle X-ray Scattering from Nickel-Neutralized Ionomers. 1. Amorphous Polymer Matrices

Richard A. Register† and Stuart L. Cooper*

Department of Chemical Engineering, University of Wisconsin, Madison, Wisconsin 53706.
Received February 28, 1989; Revised Manuscript Received May 12, 1989

ABSTRACT: Nickel-neutralized sulfonated polystyrene ionomers were examined by anomalous small-angle X-ray scattering (ASAXS) at the nickel K-edge. The intensity of the ionomer peak in the difference patterns, formed from SAXS patterns at two different energies, was shown to scale with the real part of the anomalous dispersion factor (f') and the fluorescent background with the imaginary part (f''). No change in the shape of the scattering patterns with energy was discernible, and the single-energy and difference patterns were found to be superimposable with appropriate scaling. These observations prove that both the ionomer peak and the upturn near zero angle are due to an inhomogeneous distribution of ionic repeat units throughout the material and not to precipitated neutralizing agent or microvoids. Debye plots of the intensity near zero angle were concave downward in all cases, contrary to the prediction of core-shell models of ionomer morphology.

I. Introduction

The morphology of ionomers—polymers containing a small amount of ionic functionality, typically neutralized with metal cations—has been the subject of debate for over 2 decades. By now it is generally agreed[1-3] that the often dramatic differences in material properties between ionomers and their nonionic precursors are due to the aggregation of ionic groups into microdomains, which can act as physical cross-links and ion-transport pathways in the material. The remaining dispute regards the shape and spatial arrangement of these aggregates. Because of the small size (2–10 nm) and lack of long-range order of the ionic domains, it is difficult to resolve this question by electron microscopy.[4,5] Generally, the morphology of ionomers has been probed by the small-angle scattering of X-rays (SAXS)[6-22] and neutrons (SANS).[23-25] The features that are typically observed in the scattering pattern from a phase-separated ionomer are a broad peak at a momentum transfer vector magnitude q ($q = (4\pi/\lambda)\sin\theta$, where λ is the X-ray wavelength and θ, half the scattering angle) of 0.6–3.5 nm^{-1}, as well as a strong upturn in scattered intensity as zero angle is approached, below about 0.5 nm^{-1}. The position and prominence of these features vary somewhat depending on the polymer backbone, ion content, ionic group placement, anion and cation, specimen preparation, etc. In a few cases, a shoulder on the main peak, at roughly twice the q value of the main peak, has also been reported.[8,20,22]

Several models of ionomer morphology have been proposed to account for some or all of the features in the scattering patterns. Some attribute the scattering to a dilute system of ionic aggregates having internal structure ("intraparticle" models) and postulate the existence of at least three phases with differing electron densities. These include the MacKnight core-shell model[10] and the Fujimura depleted-zone model.[17] Each models the aggregate as a spherical electron-dense core, containing a high concentration of ionic groups, which is wrapped in a layer of matrix polymer containing little or no ionic fraction. In the MacKnight model, the matrix layer is surrounded with a second spherical shell of finite thickness, composed of material containing some ionic groups but at a much lower concentration than the core. In the Fujimura model, this second shell is considered to be the continuous phase in the material and thus of infinite thickness. A third intraparticle model, proposed by Roche et al.,[11] is similar to the MacKnight model except that the aggregates consist of small trilamellar assemblies rather than spherical shells.

The interparticle models contain only a single electron density difference (aggregate – matrix) and attribute the observed intensity to interference between X-rays scattered from a concentrated system of aggregates, such as spherical aggregates residing on a simple cubic paracrystal.[7,26] Yarusso[7] proposed that the aggregates be modelled as monodisperse hard spheres with a radius of closest approach greater than their diameter, due to the necessary attachment of polymer chains to the ionic groups, with the aggregates interacting in a liquid like manner. The Yarusso model has been shown to yield a better quantitative description of the peak than either the paracrystalline or intraparticle models.[7,9]

Much less study has been devoted to the upturn near zero angle, in part because the scattering usually occurs close to the beamstop, where smearing effects from the X-ray collimation[27,28] as well as residual scattering from the collimator or beamstop are important. This has led some authors to dismiss this upturn as merely an artifact of imperfect empty beam subtraction.[7] At other times, it has been attributed to precipitated neutralizing agent or to voids or other impurities, particularly when the ionomer peak is absent.[29] In many cases, it has simply been ignored.

Anomalous small-angle X-ray scattering (ASAXS) has recently been applied to study the upturn in a nickel-neutralized sulfonated polystyrene (SPS) ionomer.[9] ASAXS makes use of the rapid change in the scattering power of an element when the energy of the incident X-rays is tuned in the vicinity of the element's absorption edges. When scattering patterns taken at different energies close to the nickel cation edge are subtracted, a "difference pattern" that reflects only the scattering from cation-containing sources can be constructed. While ASAXS has made important contributions to the study of biological macromolecules in solution[30-33] and to metallurgy,[34,35] the study referred to above[9] appears to be the only one to date on solid polymers. Those preliminary

* To whom correspondence should be addressed.
† Present address: Department of Chemical Engineering, Princeton University, Princeton, NJ 08544.

0024-9297/90/2223-0310$02.50/0 © 1990 American Chemical Society

Table I
Sample Identification

sample	% neutralization from XANES
S000	0
S050	50
S085	85
S100	92
S130	133
S170	164

results showed that the upturn was indeed related to the cation used in neutralizing the ionomer (Ni^{2+}) and not to residual camera scattering. However, the experimental error in the data was too large to ascertain whether or not the upturn and peak intensities were present in the difference pattern in the same ratio as in a single-energy pattern—that is, whether precipitated neutralizing agent or voids could be the source of the observed scattering. In addition, slight changes in the peak shape with X-ray energy, as have been found in complex colloidal systems,[38] would not have been detectable due to the relatively high noise level in the difference pattern.

The purpose of the present investigation is severalfold. Because ASAXS deals with small differences, it is essential to first ensure that the difference patterns truly result from anomalous dispersion effects and not from the inherent problems in taking a small difference of two large quantities, especially when numerous manipulations must be performed on the raw data. Second, the acquisition of more precise data allows a definitive conclusion to be drawn as to whether the ionomer peak shape changes with X-ray energy. Third, the possibility of precipitated neutralizing agent being the source of the upturn is investigated by preparing a series of ionomers with differing neutralization levels. Fourth, the possibility of voids or other impurities causing the upturn is checked by critically comparing the relative intensities of the peak and upturn in the single-energy and difference patterns. Finally, the accuracy of several previously suggested morphological models that predict an intensity increase near $q = 0$ are examined.

II. Experimental Section

A. Sample Preparation. The samples used are listed in Table I. The acid form of the sulfonated polystyrene (SPS) was generously provided by Dr. Robert Lundberg of Exxon Research and Engineering Co.; its synthesis, by post-polymerization sulfonation of polystyrene, has been described previously.[39] This material contains sulfonic acid groups at the para positions of randomly distributed styrene units; atomic absorption analysis revealed that the substitution level[7] was 6.91 mol %. Samples with varying degrees of neutralization were prepared by dissolving the polymer in tetrahydrofuran (5–10% w/w) and neutralizing with a dilute aqueous acetic acid solution of nickel hydroxide (the effective neutralizing agent is nickel acetate) to 50, 85, 100, 130, and 170% of stoichiometric. For ionomers having 100% neutralization or less, the solution was poured into 10 volumes of water at 90 °C, and the ionomer was recovered as a floc. To retain the excess neutralizing agent in the ionomers 130 and 170% neutralized, the tetrahydrofuran solvent was evaporated in air at 90 °C. All materials were dried under vacuum at 60 °C for 36 h and then at 95 °C for 24 h. Samples were compression-molded into disks at 9000 psi and 200 °C (150 °C for acid SPS sample). Some discoloration from the drying process was noted, especially for the acid and 50% neutralized specimens, but those containing Ni^{2+} exhibited predominantly that cation's characteristic green color and were transparent. Sample thicknesses were chosen to give an absorbance near unity at the nickel K-edge. The samples are denoted below by "S*xxx*", where *xxx* is the approximate percent neutralization.

B. Data Collection. The ASAXS data were collected on Beamline II-2 at the Stanford Synchrotron Radiation Laboratory, using the SSRL biotechnology camera.[9,40] For the discussion below, the important pieces of equipment are the Si(111) double-crystal monochromator with a resolution of ±4 eV, an ionization chamber before the sample serving as an incident beam monitor, an evacuated beam path, a ZnS fluorescent screen mounted in the beam stop and viewed by a photodiode serving as an after-the-sample beam monitor, and a linear position-sensitive detector of the Gabriel[41] type. The beam was collimated by sets of tantalum slits into a rectangle measuring 500 × 800 μm (parallel × perpendicular to the detection direction). The detector is positioned so that the beamstop is closer to one end than the other, but scattering patterns may still be obtained from both "ends" of the detector. The train is mounted on an optical rail to allow rapid changes of the sample-to-detector distance while retaining the alignment; scattering patterns were collected at both 50 and 30 cm. Ring currents at SSRL during this period were 30–80 mA, which provided fluxes of 900–1600 counts/s at the detector, depending on the scattering power of the sample.

By scanning the monochromator through the region of the Ni^{2+} K-edge and monitoring the ratio of ionization chamber to photodiode counts, with and without a sample in the beam, we obtained the X-ray absorption near-edge spectra (XANES) of the samples (see Figure 4). The absorption edge of a sample was defined as the midpoint of the edge jump. The edges for the samples were located approximately 0.6 eV above the edge for nickel foil, which has its edge[42] at 8332.8 eV; the edge position was rechecked periodically and found not to drift. For the SPS series, the magnitude of the edge jump was used to compute accurate degrees of neutralization; these are listed in Table I.

C. Data Reduction. As the scattered intensity changes only slightly with energy, it is essential that all relevant corrections be properly applied to the data. All data was normalized on the basis of accumulated counts in the ionization chamber. Sample transmittance was measured by comparing, at each energy, the ratio of photodiode to ionization chamber counts with and without the sample in the beam; corrections for transmittance, empty beam scattering, and thickness were than made in the standard fashion. The scattering patterns were corrected for channel-to-channel variations in detector response with the use of an ^{55}Fe source (primarily Mn Kα X-rays, 5890 eV). The channel-to-q conversion factor was obtained with a specimen of cholesterol myristate, whose 5.15-nm Bragg spacing provides three strong reflections in the range of measurement; these three reflections, plus the zero channel position, yield a detector linearity of better than 0.1%. The zero channel was found by matching the two halves of the detector response for scattering patterns from a Lupolen low-density polyethylene, which exhibits strong scattering below $q = 1$ nm^{-1}. By plotting the scattered intensity at $q = 0.42$ nm^{-1} from the Lupolen as a function of incident beam intensity (changing ring current), we determined the dead time of the detector to be 4.1 μs. This value agrees well with that found previously by beam attenuation with calibrated foils[40] and was used to apply the standard dead-time correction.[43] The data were placed on an absolute intensity scale by comparison with the calibrated[44] Lupolen's scattering, which was measured repeatedly at each energy; the absolute intensities are expressed as I/I_eV, where I_e is the intensity scattering by a single electron and V is the scattering volume. The data were smoothed with cubic splines in the upturn and peak regions and with a moving boxcar in the tail region. The data were then desmeared by the iterative method of Lake,[28,45] using the known beam length in the detection direction of 500 μm and the detector mask width of 2.65 mm. The smearing corrections were found to be negligible in the ionomer peak region but were typically 10% at the lowest accessible q value.

The 50 and 30 cm patterns for each sample were then spliced to produce curves extending from 0.18 to 5.1 nm^{-1} in q. The difference patterns were obtained by matching the tails of the patterns (4.0–5.0 nm^{-1} in the present case) to correct for the essentially isotropic[9,46] contributions from fluorescence and resonant Raman scattering.[34,47] While this procedure should produce the desired difference pattern, one additional correction

was found necessary. To test the procedure, the difference pattern of S000, which should be zero to within statistical error at all q values, was constructed. Though several fold smaller than the difference pattern for any nickel-containing material, it was not zero to within statistical error, particularly between 0.3 and 1.4 nm^{-1}. This was attributed to an apparent resonance phenomenon in the detection electronics, which caused a small oscillation (less than 1.5% pk–pk) in the detector response over this region as measured with the ^{55}Fe source. Any change in the position or amplitude of these oscillations with the X-ray energy would account for the observed effect. Thus, a small additional correction was applied by adding a fraction of the lower energy single-energy pattern to the difference pattern, the fraction being the ratio of the difference to single-energy pattern in S000 at each q value.

III. Results and Discussion

A. Anomalous Scattering Background. As the ASAXS experiment has been discussed previously,[9,30-35,38,48] only the most important elements will be reviewed here. To calculate an electron density, the atomic numbers of all atoms within a unit volume are summed. However, the effective scattering power of an element is not precisely equal to its atomic number but rather to the atomic form factor f:

$$f = f_0 + f'(E) + if''(E) \quad (1)$$

f_0 is the energy-independent term, equal to the element's atomic number. The anomalous dispersion terms f' and f'' are small compared with f_0 at most energies but can become as much as 30% of f_0 at an atomic absorption edge. The f' term becomes increasingly negative as an absorption edge is approached from lower energy, causing the element's scattering power to diminish. For the ionomers considered here, the polymer matrix has a much lower electron density than the ionic aggregates; thus, the scattered intensity diminishes as the X-ray energy approaches the cation's absorption edge. The f'' term is proportional to $E\mu(E)$, where $\mu(E)$ is the X-ray absorption coefficient[49], so f'' is small at X-ray energies below the edge; at the edge it jumps sharply and then decreases as the energy is further increased. When an X-ray energy close to, but slightly below, the absorption edge is used, the effect of f'' is to produce an isotropic intensity background due to resonant Raman scattering[34,47] and photoelectric absorption of higher energy X-rays let through by the finite band-pass of the monochromator.[46] The excess intensity background in scattering patterns taken close to the absorption edge, simply referred to as "fluorescence" below, was subtracted before constructing the difference pattern, as discussed in the Experimental Section.

SAXS patterns were generally acquired at 50 and 5 eV below the Ni^{2+} K-edge. For Ni metal,[49,50] f' changes by approximately −1.9 between these energies (f_0 = 28), which should provide sufficient contrast variation. To magnify any changes in the scattering pattern between these two energies, the lower energy pattern is subtracted from the higher energy pattern to yield a "difference pattern". For a feature to appear in the difference pattern, it must arise from scattering between cation-rich and cation-poor regions in the material. Possible rich/poor pairs would include ionic aggregates/hydrocarbon matrix, precipitated neutralizing agent/sample, and sample/microvoids, where "sample" refers to the cation content of the pure ionomer, averaged over both the ionic aggregates and the hydrocarbon matrix. As will be shown below, comparison of the single-energy and difference patterns allows discrimination between these possibilities.

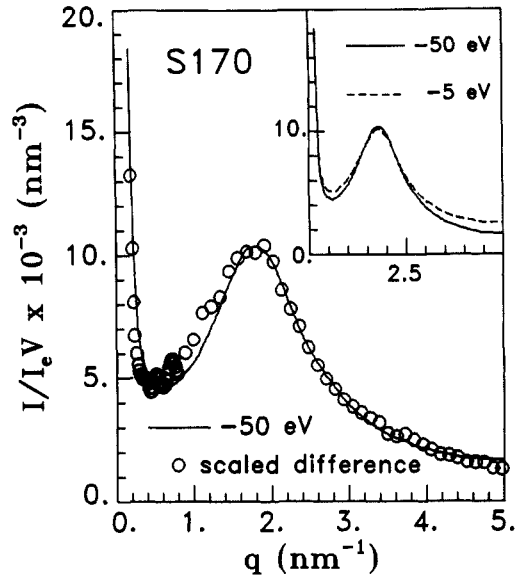

Figure 1. ASAXS data for S170. Inset: SAXS patterns taken at 50 (–) and 5 (- - -) eV below the measured Ni^{2+} K-edge. Main figure: −50 eV pattern (—) and scaled difference pattern (o) prepared from single-energy patterns in inset. Scaling required multiplication by 6.60 and addition of 1670 nm^{-3}.

B. Peak Region. The inset in Figure 1 shows how the difference pattern is obtained, using S170 as an example. The −5 eV pattern (dashed curve) contains a substantial fluorescent contribution, as can be seen in the q range of 4–5 nm^{-1}. Once this component is removed, by matching the tails of the −50 and −5 eV patterns, the peak height in the latter is less than in the former, leading to a positive peak in the difference pattern. The main portion of Figure 1 is a comparison between the −50 eV pattern and the difference pattern, which has been appropriately scaled to allow visual comparison. This scaling required multiplying the difference pattern by 6.60 and adding 1670 nm^{-3} of background scattering. These numbers were obtained by fitting the data to the Yarusso model, as described below, but could also have been obtained by trial-and-error matching of the two patterns.

There is no discernible difference in peak shape or position between the single-energy and difference patterns in Figure 1. Figure 2 further emphasizes that the shape and position of the ionomer peak in S170 do not change with energy. Here three difference patterns are presented; each is constructed from the −50 eV pattern and one taken at higher energy. The difference patterns in Figure 2 do not vary in shape; the inset shows how well the patterns superimpose when appropriately scaled. When plots are constructed analogous to Figure 1, it was found that none of the samples exhibited a change in peak shape as the X-ray energy was changed. Thus, the slight discrepancy in the morphological parameters found by Ding et al.[9] when fitting their single-energy and difference patterns to the Yarusso model may confidently be attributed to their larger experimental error.

In some respects, ASAXS is similar to performing SAXS and small-angle neutron scattering (SANS) experiments on the same sample.[51] If a material contains only two phases, the background-subtracted SAXS and SANS patterns should differ only by a constant multiple. Therefore, the superposability of the SAXS and SANS patterns can be a sensitive test of whether a material contains more than two phases, analogous to the superposability of the single-energy and difference patterns

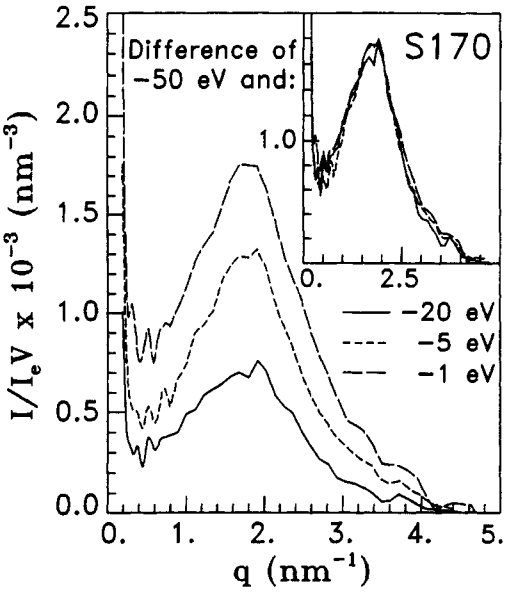

Figure 2. Difference patterns for S170. Main figure: difference between −50 eV pattern and pattern collected at (—) −20 eV, (- - -) −5 eV, and (– –) −1 eV. Inset: same, scaled (×2.36 for −20 eV, ×1.35 for −5 eV, ×1 for −1 eV).

from ASAXS. Combined SAXS and SANS have been used[52] to study an amorphous, cesium-neutralized poly(ethylene-*co*-methacrylic acid), wherein it was found that the ratio of upturn to peak intensity observed by SANS was much greater than that observed by SAXS. The lack of superposability was cited in support of the three-phase lamellar model of Roche et al.[11]

However, each of the two ion-rich phases in the three-phase models (core and shell or inner and outer lamellae) achieves its enhanced electron density (or scattering length density) solely because of a greater *number* density of ionic groups in that phase than in the ion-poor regions, if volume additivity is a good approximation. Put another way, if a multiphase material contains only two components (e.g., ionic and hydrocarbon repeat units), then no matter how many phases are present or how the two components partition between the phases, the SAXS and SANS patterns (or single-energy and difference ASAXS patterns) should always be superposable if volume additivity is obeyed. For the sodium salts of other poly(ethylene-*co*-methacrylic) acids, volume additivity has been shown to hold[53] within 0.5%. Thus, while the superposability of the single-energy and difference ASAXS patterns observed here is consistent with a two-phase interparticle model, it does not rule out the three-phase intraparticle models. The apparent contradiction between the good superposability found here and the poor superposability found by Roche et al.[52] may be explained by the presence of third component in the latter experiments, namely, the "foreign heterogeneities" that were observed to cause strong scattering at low q even in the acid form of the polymer,[29] which contains no aggregates.

As detailed in the Experimental Section, numerous corrections had to be applied to the data to ensure that the intensities of the single-energy patterns were as accurate as possible. It is important to show, then, that the difference patterns presented in Figures 1 and 2 derive from anomalous effects and not from artifacts of the data treatment. Figures 3 and 4 demonstrate that the former is truly the case. Changing f' is manifested in the height of the ionomer peak in the difference pattern. For an interparticle interference model, the peak height above background in a single-energy pattern is proportional to

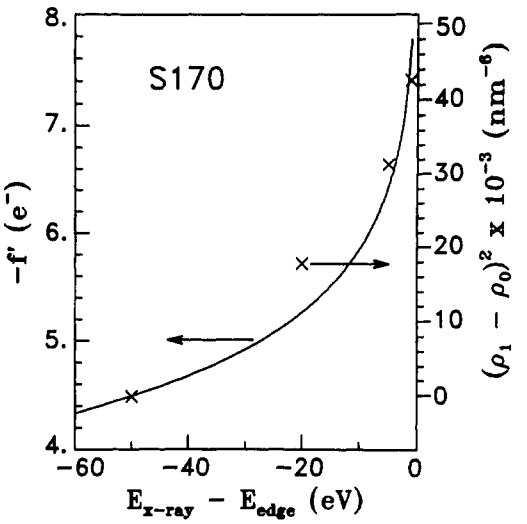

Figure 3. Scaling test, S170 ionomer peak intensity with f'. Left scale and (—): curve for nickel metal based on data of Suortti et al.[50] Right scale and (×): squared electron density differences based on Yarusso model.

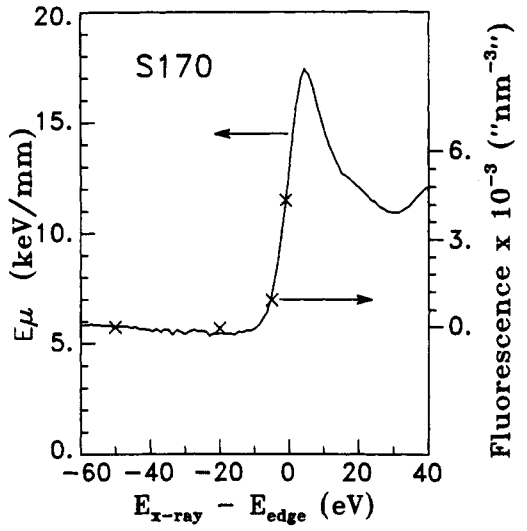

Figure 4. Scaling test, fluorescent background with $E\mu(E)$. Left scale and (—): experimental value of $E\mu$ for S170 from near-edge spectrum. Right scale and (×): fluorescent background intensity.

the square of the difference between the ionic aggregate electron density ρ_1, and the matrix electron density ρ_0. (For the MacKnight, Roche, or Fujimura models, the intensity expression is more complicated but is still proportional to the square of the electron density difference between ionic and hydrocarbon repeat units. Thus, the argument presented here does not hinge on the choice of model.) At energies below the edge, where f' effects dominate, we may write

$$(\rho_1 - \rho_0) = a(b + f') \tag{2}$$

where a is a proportionality constant and b represents the nonanomalous part of the electron density difference between aggregates and matrix (which includes contributions from such sources as sulfonate groups and the f_0 portion of the nickel atomic form factor). Thus, if we denote the f' values at energies 1 and 2 by subscripts, the electron density difference in a difference pattern (dp) is

$$(\rho_1 - \rho_0)_{dp}^2 = a^2(2b(f'_1 - f'_2) + [(f'_1)^2 - (f'_2)^2]) \tag{3}$$

Even at the edge, the ionic aggregates still have an effec-

Table II
Yarusso Model Parameters for S170 Patterns

pattern,[a] eV	R_1,[b] nm	R_2/R_1[b]	v_p,[b] nm^3	$\rho_1 - \rho_0$, nm^{-3}
-50	0.81	1.91	82	461
-50/-20				134
-50/-5				177
-50/-1				206

[a] Dual-numbered patterns refer to difference patterns taken between the two energies indicated. [b] Fixed for all difference patterns at the value computed for the -50 eV pattern.

tive electron density much higher than the matrix, so b is always much larger than f'. thus, the second term on the right-hand side may be neglected to a first approximation, and $(\rho_1 - \rho_0)_{dp}^2$ should be linearly related to f'. The difference patterns for S170 were used to test the f' scaling given by eq 3.

Since $(\rho_1 - \rho_0)_{dp}^2$ is proportional to the height of the ionomer peak, we could simply test whether the peak height is linearly related to f'. However, taking a single-point measurement of peak height in the presence of experimental noise and a varying background level is not the optimal way to treat the data. It is preferable to use least-squares fitting to an analytical representation for the peak to determine the best values of the background level (artificially set negative in matching the tails of the single-energy patterns) and the peak height above background. For this purpose, we selected the Yarusso model with the Percus–Yevick interference function.[7,9,54-57] The modelling parameters are shown in Table II; R_1 is the radius of the ionic aggregate, R_2 the radius of closest approach between aggregates, and v_p the total volume of material per ionic aggregate. In the fits to the difference patterns, the parameters determining the shape of the curve (R_1, R_2, and v_p) were fixed at the values found for the -50 eV pattern.

Values of f' for Ni^{2+} are not available for comparison with $(\rho_1 - \rho_0)_{dp}^2$, but f' for Ni^0 (metal) has been measured by several investigators. The data of Suortti et al.,[50] obtained by absolute intensity measurements of crystal reflections, is well-represented over the range of interest by

$$\log (f') = -7.774 + 1.934 \log (E_{edge} - E_{X\text{-}ray}) \quad (4)$$

This curve and the $(\rho_1 - \rho_0)_{dp}^2$ values are plotted in Figure 3; the superposition is reasonably good. While some of the discrepancy may be due to experimental error, some is also due to differences in f' between Ni^{2+} and Ni^0. Since f' and f'' are related by the Kramers–Kronig relations and f'' is proportional to $E\mu(E)$ as measured by the XANES spectra and the XANES spectra for Ni foil and for the ionomer samples differ markedly, it is clear that some differences in f' between Ni^0 and Ni^{2+} do exist.

An analogous test may be made for the effects of f'' by superimposing the "fluorescent" background intensity on a plot of $E\mu(E)$ computed from the XANES spectrum, as shown in Figure 4. The superposition is excellent here, since the f'' data (whose surrogate in Figure 4 is $E\mu(E)$) were obtained for the actual sample under study and not for Ni foil. Thus, it is clear that the effects observed here truly arise from anomalous dispersion and are not artifacts of the data treatment.

Figure 5 shows the -50 eV patterns for the entire SPS series; that for S085 is virtually identical with that for S100. As the degree of neutralization increases, the peak intensity increases while the upturn intensity decreases; in S170, the upturn is nearly an order of magnitude weaker than in the acid SPS. This confirms that the upturn is

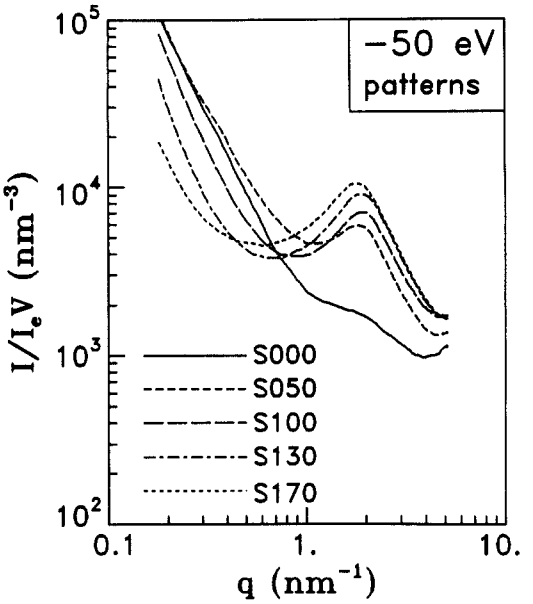

Figure 5. -50 eV patterns for sulfonated polystyrene ionomers: (–) S000, (- - -) S050, (– –) S100, (– - –) S130, (···) S170.

not due to precipitated particles of nickel acetate, as the upturn would not then be present in S000 and would also be expected to increase dramatically in intensity for neutralization levels above stoichiometric. Moreover, since the peak intensity continues to increase beyond 100% neutralization, this indicates that at least some of the excess neutralizing agent incorporates itself into the ionic aggregates, as has been generally assumed.[58]

S000 (acid SPS) exhibits a weak ionomer peak; this point has been the subject of some controversy, with one group reporting its presence[7] and another its absence[14,15] even in samples prepared similarly. The latter group has attributed the discrepancy to the presence in the acid aggregates of residual dimethyl sulfoxide, used by the former group in the solution from which they precipitated their polymer. In the present case, only tetrahydrofuran and water were used, indicating that the scattering contrast between sulfonic acid groups and polystyrene is sufficient to produce an observable peak.

Since none of the ionomers exhibited a change in peak shape with energy, an analysis similar to that carried out in preparing Figure 3 can be used on all the SPS samples to see how the relative importance of the anomalous effects changes with the degree of neutralization. The parameter examined here is the ratio of $(\rho_1 - \rho_0)_{dp}$ to $(\rho_1 - \rho_0)$ at 50 eV below the edge; roughly, the square root of the ratio of peak intensities in the difference and single-energy patterns. This ratio must be zero at 0% neutralization, as no nickel is present but the scattering peak is visible; as the degree of neutralization increases, the ratio would be expected to reach a plateau as the aggregates approach pure nickel acetate in composition. The parameters obtained from the Yarusso model are listed in Table III, while Figure 6 shows the ratio plotted against the degree of neutralization. The dashed curve is simply a guide to the eye. The data appear to describe a curve having the expected shape, and the ratio appears to plateau at approximately 0.4. Using the f' values of Suortti for Ni^0 and assuming that the limiting case at high neutralization is a dispersion of nickel acetate tetrahydrate in polystyrene, we expected the limiting value to be 0.28. Since f' for Ni^{2+} and Ni^0 differ and the trend shown in Figure 6 is as expected, this should be considered reasonable agreement.

Table III
Yarusso Model Parameters for SPS Samples

sample	fit range,[a] nm^{-1}	R_1,[b] nm	R_2/R_1[b]	v_p,[b] nm^3	$\rho_1 - \rho_0$, nm^{-3}
S000	1.6–5	0.77	2.05	153	252
	diff				82
S050	1.2–5	0.84	1.79	83	312
	diff				82
S085	1.0–5	0.79	1.83	64	341
	diff				110
S100	1.0–5	0.80	1.84	66	345
	diff				106
S130	0.8–5	0.78	1.92	68	435
	diff				166
S170	0.6–5	0.81	1.91	82	461
	diff				177

[a] First line for each specimen contains the results for the −50 eV pattern; second line is for the difference pattern, using the same fit range and R_1, R_2, and v_p values as found for the −50 eV pattern. [b] Fixed for all difference patterns at the value computed for the −50 eV pattern.

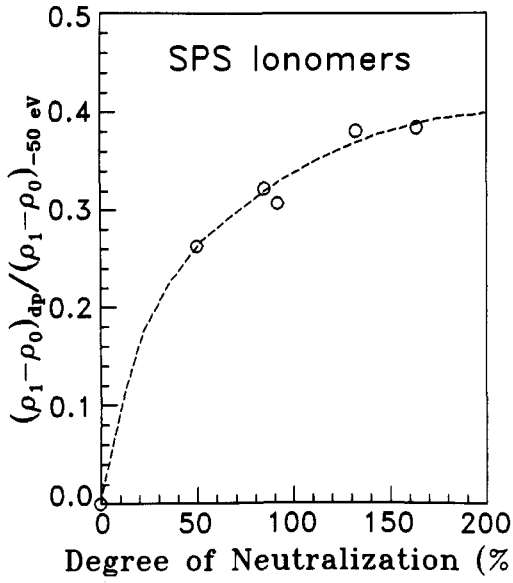

Figure 6. Ratio of electron density differences between difference and single-energy patterns (O). Dashed line is a guide to the eye.

It should also be noted that the $(\rho_1 - \rho_0)$ values listed in Table III are quite large; as polystyrene has ρ_0 = 340 e/nm^3, these correspond to ρ_1 values ranging from 592 to 801 e/nm^3. For comparison, $Ni(CH_3COO)_2 \cdot 4H_2O$ has an electron density of 566 e/nm^3, while $NiSO_4 \cdot 6H_2O$ has an electron density of 645 e/nm^3. This suggests that the model overestimates the value of ρ_1. (For comparison, the following paper[59] shows that ρ_1 in dry Nafion perfluorosulfonate membranes is about 580 e/nm^3.) The difficulty is that the model is not very sensitive to the value of R_1; for instance, a value of R_1 = 0.95 nm for S170 yields a value of ρ_1 = 622 e/nm^3 and nearly as good a fit. This point is explored in greater detail elsewhere;[60] however, it does not affect the ratio plotted in Figure 6.

C. Upturn Region. The intensity upturn at low angles has variously been dismissed as the result of residual camera scattering,[7] voids or impurities,[29] or precipitated neutralizing agent.[7,9] In the present study, the data were truncated at a q value well above that where significant residual camera scattering occurs, which rules out the first source. The scattering patterns shown in Figure 5 have already eliminated precipitated neutralizing agent as a possibility. Since all the samples were prepared from the same acid SPS, if the upturn were due to foreign

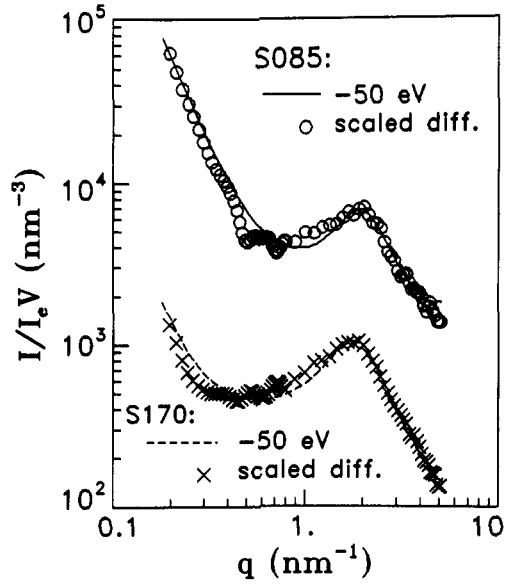

Figure 7. S085: −50 eV (—) and scaled difference (O) patterns, S170: −50 eV (- - -) and scaled difference (×) patterns. Intensities for S170 have been lowered by one log unit. Scaling for S085 difference pattern: ×9.63, +1600 nm^{-3}.

heterogeneities, it should appear with approximately the same intensity regardless of the degree of neutralization. Instead, its intensity decreases smoothly with increasing neutralization, eliminating impurities as a substantial source of upturn scattering here. Voids still remain a possible explanation, however, and will be addressed next.

Figure 7 shows the −50 eV and scaled difference patterns for S085 and S170 on a log–log scale; those for S170 have been shifted downward by one log intensity unit, for clarity. For these as well as the other samples, the −50 eV and difference patterns have the same shape over the entire q range, within experimental error. Were the upturn due to voids, it would not be totally absent in the difference pattern, since the effective electron density of the pure ionomer (averaged over both aggregates and matrix) would diminish slightly. However, most of the scattering contrast between voids and sample arises from the electron density of the hydrocarbon matrix, so changes in the scattering power of Ni^{2+} would have only a small effect on the sample–void contrast. On the other hand, since the aggregate–matrix contrast is due exclusively to a difference in the number density of Ni^{2+} cations between the two phases, changes in the scattering power of Ni^{2+} would have a strong effect on the intensity of the ionomer peak. The fact that the single-energy and scaled difference patterns superpose well unambiguously rules out voids as the source of scattered intensity near zero angle.

It has also been suggested that the upturn is due to a nonrandom distribution of the unaggregated ionic groups (small multiplets or "dissolved" ionic groups) residing within the matrix.[9] This explanation is not at odds with the present results, for the same reason that the superposability cannot distinguish between the interparticle and intraparticle models. A similar hypothesis would be to assume that there is an inhomogeneous distribution of ionic aggregates within the sample, such as in finite paracrystalline lattices separated by aggregate-free regions.[29] However, the lack of nonionic matrix chains to fill these regions makes the physical basis of such a model rather tenuous. It has also been suggested[9] that the shape of the upturn can be described by the Debye–Bueche ran-

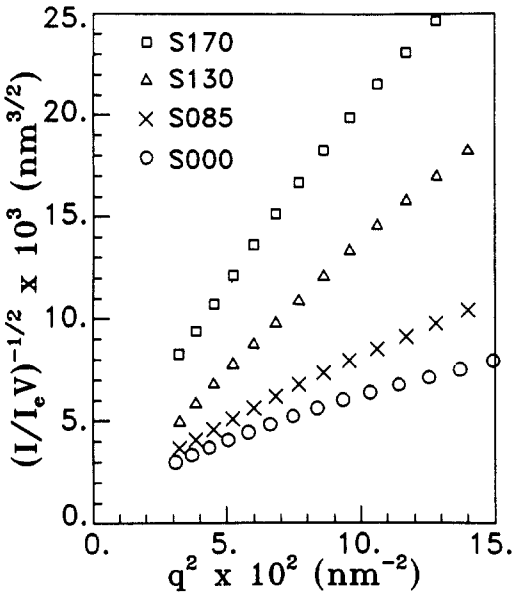

Figure 8. Debye plots for upturn region of sulfonated polystyrene ionomers: (○) S000, (×) S085, (△) S130, (□) S170.

dom-two-phase model[36,37]

$$I/I_eV = 8\pi\phi(1-\phi)(\Delta\rho)^2/c(q^2 + c^{-2})^2 \quad (5)$$

where ϕ is the volume fraction of either the ion-rich or ion-poor portion of the matrix, $\Delta\rho$ is the electron-density difference between the two types of region, and c is the correlation length, a measure of the size of the regions. According to the above equation, a Debye plot ($I^{-1/2}$ vs q^2) of the intensity above background should yield a straight line. If this explanation is correct, then the "background" in the upturn region consists of two contributions: (1) the true SAXS background, due to the leading edge of wide-angle scattering, fluorescence, thermal density fluctuations, mixing of matrix matter into the ionic aggregates, and ionic groups dissolved in the matrix, and (2) the leading edge of the ionomer peak intensity, which would then be described by the Yarusso model.[9]

Since the single-energy and difference patterns have the same shape, we can use the single-energy patterns (which possess much better counting statistics) to test this hypothesis. The first source of background was found by fitting the tail region of the curves (3–5 nm^{-1}) to Porod's law[61] plus a Vonk-like background[62] of the type $(I/I_eV)_b = A + Bq^4$. The Bq^4 term arises from the leading edge of a polystyrene wide-angle reflection[63] at 7 nm^{-1}; B was found from the S000 data and held fixed for the other samples. The curves with $(I/I_eV)_b$ subtracted were fit with the Yarusso model, yielding the parameter values in Table III. The Yarusso model fits were subtracted from the data, and the residuals were recast in the Debye format to yield Figure 8. (The curves for S000 and S050 and for S085 and S100 nearly superimpose, so only one from each pair is shown.) Fortunately, the upturn intensity is large enough that it is rather insensitive to any errors in background subtraction. In all cases, the Debye plots do not describe straight lines, even at the lowest accessible q values. While it might be argued that the plots would straighten out if lower q values were attained, very recent data[13] on other SPS ionomers reveals that the curvature persists to at least 0.03 nm^{-1}. Thus, the Debye–Bueche model is an unsatisfactory quantitative representation for the upturn; all the Debye plots are concave downward.

One obvious shortcoming of the Yarusso model is that it does not predict an upturn in scattered intensity near zero angle. The MacKnight, Roche, and Fujimura models do predict an upturn, which is often cited in their favor. The MacKnight and Fujimura models behave as Rayleigh functions[64] near $q = 0$, and the Roche model is similar; therefore, all three models predict Debye plots with a pronounced upward concavity, in disagreement with the results shown in Figure 8. Thus, none of the morphological models proposed to date is completely satisfactory. One possibility that has not been explored in detail is to introduce an attractive potential between the ionic aggregates in the Yarusso model, which results in both a peak and an upturn;[65] this model will be discussed in detail elsewhere.[60]

IV. Conclusions

Nickel-neutralized sulfonated polystyrene ionomers of varying neutralization level were studied by ASAXS at the Ni^{2+} K-edge. The single-energy and difference patterns were found to be superimposable in all cases, with appropriate scaling, and no change in the shape of the scattering patterns with energy was discernible. These observations unambiguously show that both the ionomer peak and the low-q upturn are due to an inhomogeneous distribution of ionic repeat units in the samples and not to precipitated neutralizing agent or voids. The intensity of the ionomer peak was found to scale with f', while the fluorescent contribution was found to scale with f'', demonstrating that the difference patterns truly arise from anomalous effects and not from artifacts of the data treatment. The peak height increased and the upturn intensity decreased with increasing neutralization, with no abrupt change at the stoichiometric point, indicating that the excess neutralizing agent is taken up by the ionic aggregates. Finally, Debye plots of the intensity near zero angle were found to be concave downward in all cases examined, contrary to the predictions of the intraparticle interference models proposed to date.

Acknowledgment. R.A.R. wishes to thank Prof. Keith O. Hodgson for the opportunity to conduct these ASAXS experiments. The assistance of Drs. Stevan R. Hubbard and Soichi Wakatsuki was invaluable in setting up the camera and collecting and transferring the data, and they provided many helpful discussions as well. Y. S. Ding also assisted in the data collection. Support for this work was provided by the U.S. Department of Energy through Grant DE-FG02-88ER45370; by the donors of the Petroleum Research Fund, administered by the American Chemical Society; and by a fellowship for R.A.R. from the Fannie and John Hertz Foundation. The Stanford Synchrotron Radiation Laboratory is supported by the Department of Energy, Office of Basic Energy Science, and the National Institutes of Health, Biotechnology Resources Program, Division of Research Resources.

References and Notes

(1) MacKnight, W. J.; Earnest, T. R. *Macromol. Rev.* **1981**, *16*, 41.
(2) Eisenberg, A., Bailey, F. E., Eds. *Coulombic Interactions in Macromolecular Systems*; ACS Symposium Series 302; American Chemical Society; Washington, 1986.
(3) Pinéri, M.; Eisenberg, A. *Structure and Properties of Ionomers*; NATO ASI Series C 198; D. Reidel: Boston, 1987.
(4) Handlin, D. L.; MacKnight, W. J.; Thomas, E. L. *Macromolecules* **1981**, *14*, 795.
(5) Li, C.; Register, R. A.; Cooper, S. L. *Polymer* **1989**, *30*, 1227.
(6) Marx, C. L.; Caulfield, D. F.; Cooper, S. L. *Macromolecules* **1973**, *6*, 344.

(7) Yarusso, D. J.; Cooper, S. L. *Macromolecules* **1983**, *16*, 1871.
(8) Lee, D.-c.; Register, R. A.; Yang, C.-z.; Cooper, S. L. *Macromolecules* **1988**, *21*, 998.
(9) Ding, Y. S.; Hubbard, S. R.; Hodgson, K. O.; Register, R. A.; Cooper, S. L. *Macromolecules* **1988**, *21*, 1698.
(10) MacKnight, W. J.; Taggart, W. P.; Stein, R. S. *J. Polym. Sci., Polym. Symp.* **1974**, *45*, 113.
(11) Roche, E. J.; Stein, R. S.; Russell, T. P.; MacKnight, W. J. *J. Polym. Sci., Polym. Phys. Ed.* **1980**, *18*, 1497.
(12) Chu, B.; Wu, D.-Q.; MacKnight, W. J.; Wu, C.; Phillips, J. C.; LeGrand, A.; Lantmann, C. W.; Lundberg, R. D. *Macromolecules* **1988**, *21*, 523.
(13) Wu, D. Q.; Phillips, J. C.; Lundberg, R. D.; MacKnight, W. J.; Chu, B. *Macromolecules* **1989**, *22*, 992.
(14) Peiffer, D. G.; Weiss, R. A.; Lundberg, R. D. *J. Polym. Sci., Polym. Phys. Ed.* **1982**, *20*, 1503.
(15) Weiss, R. A.; Lefelar, J. A. *Polymer* **1986**, *27*, 3.
(16) Galambos, A. F.; Stockton, W. B.; Koberstein, J. T.; Sen, A.; Weiss, R. A.; Russell, T. P. *Macromolecules* **1987**, *20*, 3091.
(17) Fujimura, M.; Hashimoto, T.; Kawai, H. *Macromolecules* **1981**, *14*, 1309.
(18) Fujimura, M.; Hashimoto, T.; Kawai, H. *Macromolecules* **1982**, *15*, 136.
(19) Gebel, G.; Aldebert, P.; Pinéri, M. *Macromolecules* **1988**, *20*, 1425.
(20) Broze, G.; Jérôme, R.; Teyssié, P.; Gallot, B. *J. Polym. Sci., Polym. Lett. Ed.* **1981**, *19*, 415.
(21) Williams, C. E.; Russell, T. P.; Jérôme, R.; Horrion, J. *Macromolecules* **1986**, *19*, 2877.
(22) Horrion, J.; Jérôme, R.; Teyssié, P.; Marco, C.; Williams, C. E. *Polymer* **1988**, *29*, 1203.
(23) Roche, E. J.; Pinéri, M.; Duplessix, R.; Levelut, A. M. *J. Polym. Sci., Polym. Phys. Ed.* **1981**, *15*, 1390.
(24) Earnest, T. R.; Higgins, J. S.; MacKnight, W. J. *Macromolecules* **1982**, *15*, 136.
(25) Clough, S. B.; Cortelek, D.; Nagabhushanam, T.; Salamone, J. C.; Watterson, A. C. *Polym. Eng. Sci.* **1984**, *24*, 385.
(26) Hosemann, R.; Bagchi, S. N. *Direct Analysis of Diffraction by Matter*; North-Holland: Amsterdam, 1962.
(27) Hendricks, R. W.; Schmidt, P. W. *Acta Phys. Austriaca* **1967**, *37*, 20.
(28) Register, R. A.; Cooper, S. L. *J. Appl. Crystallogr.* **1988**, *21*, 550.
(29) Roche, E. J. Ph.D. Thesis, University of Massachusetts, 1978.
(30) Lye, R. C.; Phillips, J. C.; Kaplan, D.; Doniach, S.; Hodgson, K. O. *Proc. Natl. Acad. Sci. U.S.A.* **1980**, *77*, 5884.
(31) Miake-Lye, R. C.; Doniach, S.; Hodgson, K. O. *Biophys. J.* **1983**, *41*, 287.
(32) Fairclough, R. H.; Miake-Lye, R. C.; Stroud, R. M.; Hodgson, K. O.; Doniach, S. *J. Mol. Biol.* **1986**, *189*, 673.
(33) Stuhrmann, H. B. *Adv. Polym. Sci.* **1985**, *67*, 123.
(34) Goudeau, P.; Fontaine, A.; Naudon, A.; Williams, C. E. *J. Appl. Crystallogr.* **1986**, *19*, 19.
(35) Goudeau, P.; Naudon, A.; Chamberod, A.; Rodmacq, B.; Williams, C. E. *Europhys. Lett.* **1987**, *3*, 269.
(36) Debye, P.; Bueche, A. M. *J. Appl. Phys.* **1949**, *20*, 518.
(37) Debye, P.; Anderson, H. R.; Brumberger, H. *J. Appl. Phys.* **1957**, *28*, 679.
(38) Williams, C. E.; Derian, P. J.; Warr, G. G. *Polym. Prepr. (Am. Chem. Soc., Div. Polym. Chem.)* **1988**, *29*(1), 373.
(39) Makowski, H. S.; Lundberg, R. D.; Singhal, G. H. U.S. Patent 3 870 841, 1975, to Exxon Research and Engineering Co.
(40) Hubbard, S. R. Ph.D. Thesis, Stanford University, 1987.
(41) Gabriel, A. *Rev. Sci. Instrum.* **1977**, *48*, 1303.
(42) Weast, R. C., Ed. *CRC Handbook of Chemistry and Physics*, 59th ed.; CRC Press: Boca Raton, FL, 1978; p E-192.
(43) Alexander, L. E. *X-Ray Diffraction Methods in Polymer Science*; Wiley-Interscience: New York, 1970; p 117.
(44) Pilz, I.; Kratky, O. *J. Colloid Interface Sci.* **1967**, *24*, 211.
(45) Lake, J. A. *Acta Crystallogr.* **1967**, *23*, 191.
(46) Aur, S.; Kofalt, D.; Waseda, Y.; Egami, T.; Chen, H. S.; Teo, B.-K.; Wang, R. *Nucl. Instrum. Methods Phys. Res., Sect. A* **1984**, *222*, 259.
(47) Eisenberger, P.; Platzman, P. M.; Winick, H. *Phys. Rev. B* **1976**, *13*, 2377.
(48) James, R. W. *The Optical Principles of the Diffraction of X-Rays* Cornell University Press: Ithaca, New York, 1965.
(49) Bonse, U.; Hartmann-Lotsch, I. *Nucl. Instrum. Methods Phys. Res., Sect. A* **1984**, *222*, 185.
(50) Suortti, P.; Hastings, J. B.; Cox, D. E. *Acta Crystallogr. A* **1985**, *A41*, 417.
(51) Schelten, J.; Hendricks, R. W. *J. Appl. Crystallogr.* **1978**, *11*, 297.
(52) Roche, E. J.; Stein, R. S.; MacKnight, W. J. *J. Polym. Sci., Polym. Phys. Ed.* **1980**, *18*, 1035.
(53) Marx, C. L.; Cooper, S. L. *Makromol. Chem.* **1973**, *168*, 339.
(54) Percus, J. K.; Yevick, G. *Phys. Rev.* **1958**, *110*, 1.
(55) Wertheim, M. S. *Phys. Rev. Lett.* **1963**, *10*, 321.
(56) Thiele, E. *J. Chem. Phys.* **1963**, *39*, 474.
(57) Kinning, D. J.; Thomas, E. L. *Macromolecules* **1984**, *17*, 1712.
(58) Bagrodia, S.; Wilkes, G. L. *Polym. Eng. Sci.* **1986**, *26*, 662.
(59) Register, R. A.; Cooper, S. L. *Macromolecules*, following paper in this issue.
(60) Register, R. A. Ph.D. Thesis, University of Wisconsin—Madison, 1989.
(61) Porod, G. *Kolloid-Z.* **1951**, *124*, 83.
(62) Vonk, C. G. *J. Appl. Crystallogr.* **1971**, *4*, 70.
(63) Song, H. H.; Roe, R. J. *Macromolecules* **1987**, *20*, 2723.
(64) Rayleigh, Lord *Proc. R. Soc. London, A* **1914**, *A90*, 219.
(65) Fournet, G. *Acta Crystallogr.* **1951**, *4*, 293.